

Numerical study of the ground-state properties of a frustrated XY model

P. Gawiec and D. R. Grempel

*Centre d'Etudes Nucléaires de Grenoble, Département de Recherche Fondamentale, Service de Physique,
Laboratoire de Magnétisme et Diffraction Neutronique, 85X, F-38041 Grenoble CEDEX, France*

(Received 19 February 1991)

We study numerically the ground-state morphology and properties of the low-lying states of an XY model with competing interactions for several values of the concentration x and of the ratio between ferromagnetic and antiferromagnetic exchange constants, λ . If $\lambda > 1$, the ground state is likely to be a spin glass for all nonzero concentrations. In the region $\lambda \leq 1$, the ground state is a disordered canted ferromagnet for low dilutions with a transition to a pure spin-glass phase at a λ -dependent critical concentration. The analysis of the spin-spin correlation functions gives insight on the mechanism responsible for the degradation of the magnetic order at low dilutions. An unusual law of decay of correlations suggests that the canted ferromagnetic phase that we find at small λ and x may actually be a phase with power-law decay of correlations.

I. INTRODUCTION

In this paper we study numerically the ground-state morphology of a disorder XY model on a two-dimensional square lattice where the host ferromagnetic bonds of strength J are diluted by antiferromagnetic bonds $-\lambda J$ present with concentration x . This and related frustrated models have been used to describe the properties of diluted ferromagnetic systems such as amorphous magnets^{1,2} and spin glasses.²⁻⁵ There has been a renewed interest in this model Hamiltonian since the recent suggestion that it could be relevant for the interpretation of the magnetic properties of the Cu-based high-temperature superconducting materials in the insulating phase.⁶

The determination of the ground-state structure of this model constitutes an interesting and nontrivial problem because, in contrast with the more extensively studied random Ising models, in a vector model, besides the direct short-range interactions between spins, there exist host-mediated long-range interactions between defects of the ferromagnetic structure that play an important role in the problem, notably at low concentrations.

The effect of these interactions has been discussed in recent papers by Vannimenus *et al.*⁷ and by Saslow and Parker.^{1,8} These authors have analyzed the conditions of stability of the ferromagnetic state in the presence of one and two impurities by numerical and analytical methods. For one impurity and $\lambda \leq 1$, the ferromagnetic state is locally stable. The instability threshold λ_c for two antiferromagnetic bonds decreases as a result of impurity interactions and its value depends upon the distance between defects and their relative orientation. Beyond threshold, the long-distance spin-distortion pattern is dipolar and its amplitude, determined by nonlinear terms, vanishes as $\lambda \rightarrow \lambda_c$. It will be seen below that one can find similar effects in three- and four-impurity clusters.

For a finite concentration x of impurities, no exact analytic calculation is possible and one must resort to approximations and numerical simulations to get informa-

tion about the different phases of the model.

The coherent potential approximation (CPA) has been used⁷ to study the $T=0$ phase diagram. According to the CPA, there exists a line $\lambda_c(x)$ in the x - λ plane that separates a region where the ferromagnetic state is stable from another where large-scale spin deviations set in. The line is such that the region $\lambda \geq 1$ lies entirely in the unstable region. This instability of the ferromagnetic state is signaled by the appearance of a pole at negative energy in the scattering matrix of a spin wave propagating in the disordered medium. In the CPA scheme, the T matrix is calculated neglecting interference between waves multiply scattered by different bonds. This is unlikely to be a good approximation here because the results for small clusters quoted above suggest that collective effects are important. However, if interpreted with caution,⁷ the CPA results can be of qualitative value. The existence of clusters of all sizes and shapes makes the collinear state unstable for all λ and $x \neq 0$ in the thermodynamic limit. As a consequence, a naive interpretation of the CPA curve, as indicating the onset of noncollinearity, is incorrect, quite likely, λ_c approximately describes the crossover line from a regime where the noncollinearity is small to another where it is large,⁷ one cannot exclude *a priori* an interpretation in terms of a transition from a magnetic to a nonmagnetic state.

Besides its difficulties of interpretation, the CPA cannot describe in detail the structure of the disordered ferromagnetic phase or address the problem of an eventual transition between this phase and a spin-glass state. These questions require numerical investigation and constitute the main motivation of this work.

One can use physical arguments together with the results for small clusters of impurities to infer how the phase diagram should look like at $T=0$. Locally, the competition between ferro- and antiferromagnetic bonds favors spin canting. We may thus expect that, for small λ and small to moderate x , the instability of the ferromagnetic state will be to a noncollinear state with reduced magnetization. For large enough λ , on the other hand, a

pure spin-glass phase without magnetic long-range order seems more likely at all concentrations. This stems from the fact that, if λ is large enough, individual impurity bonds induce a distortion. As first shown by Villain,⁹ in the canted state, a local chiral symmetry, nonexistent in the ferromagnetic state, is broken. The discrete degeneracy introduced by local chiral symmetry breaking may be described by attaching an Ising-like internal degree of freedom, or pseudospin, to every defect. Long-range interactions between pseudospins lift the degeneracy and may give rise to the appearance of a disordered spin-glass phase.

In order to study these issues we have performed a detailed numerical investigation of the $T=0$ morphology of finite but fairly large systems covering the whole range of concentrations and several typical values of λ . We have developed an efficient algorithm to generate sets of low-energy quasidegenerate states which we use to study the various order parameters that characterize the possible ground states and the spin-spin correlation functions.

An unbiased interpretation of our results for the order parameters supports the picture proposed above. Our data suggest that, in the region $\lambda < 1$, at low concentration, the system is a disordered canted ferromagnet with spin-glass ordering in the transverse component of the spin and undergoes a transition to a spin-glass state at a critical concentration $x_c(\lambda)$ where the magnetization vanishes. Interpretation of the results for $\lambda \geq 1$ is less straightforward. Whereas the data are consistent with a spin-glass phase with zero magnetization for $x \neq 0$, they do not completely rule out the possibility that there are two phases just as for $\lambda < 1$ with $x_c(\lambda)$ a rapidly decreasing function.

The results for the spin-spin correlations are somewhat surprising because they reveal an unusual form for the decay of correlations at low concentrations. They suggest that one should seriously examine the possibility that the low-concentration, low λ , phase that we identify as being a canted ferromagnet is, in reality, a phase with algebraic decay of correlations.

II. METHODOLOGY AND MORPHOLOGY OF GROUND STATES

We consider the model Hamiltonian

$$H = - \sum_{\langle i,j \rangle} J_{i,j} \mathbf{S}_i \cdot \mathbf{S}_j, \quad (1)$$

where \mathbf{S}_i is a planar spin, $|\mathbf{S}_i| = 1$, and

$$J_{i,j} = \begin{cases} J, & \text{with probability } 1-x, \\ -\lambda J, & \text{with probability } x. \end{cases} \quad (2)$$

The summation in (1) is restricted to distinct nearest-neighbor pairs. The configurations that minimize the energy (1) obey the equations

$$\mathbf{S}_i = \frac{\mathbf{H}_i}{|\mathbf{H}_i|}, \quad (3a)$$

$$\mathbf{H}_i = \sum_j J_{i,j} \mathbf{S}_j. \quad (3b)$$

These equations express that, in equilibrium, each spin must lie in the direction of the internal magnetic field at its site. To solve the system (3a) and (3b), one usually starts from some initial random configuration and sequentially rotates the spins into the direction of their local field. Since, as a result of each move, the local fields themselves change, the procedure is repeated a large number of times until convergence.^{3,10}

Quite aside from the fact that (3a) and (3b) are necessary but not sufficient conditions for a configuration to be a minimum,¹¹ this method is not a particularly efficient way of locating ground states. If we think in terms of configuration space, we see that this algorithm takes us from an initial configuration to a stationary one along a path composed of a sequence of straight segments along each of which the orientation of one spin varies while the rest are held fixed. It will be clear below that this path is far from being the optimal one for our problem. We have devised a procedure based on the conjugate gradient method,¹² an algorithm that is both well suited for our purposes and relatively simple to implement. It differs from the more naive method in that the path to the minimum is not fixed *a priori* but is chosen at each step of the iteration in order to improve the rate of convergence to a local minimum. A most important feature is that it includes the possibility of a simultaneous adjustment of clusters of spins of arbitrary size.

We illustrate the procedure with data from a 20×20 system with $\lambda = 0.5$ and $x = 0.2$. Figure 1 shows, in the form of a scatter plot (energy versus magnetization), stationary states reached by starting the minimization procedure from 50 different random initial conditions, each of which evolved into a different minimum. Figure 1 exhibits an important feature of this model, namely, the existence of sets of states that lie very close in energy but have widely different magnetizations. This reflects the

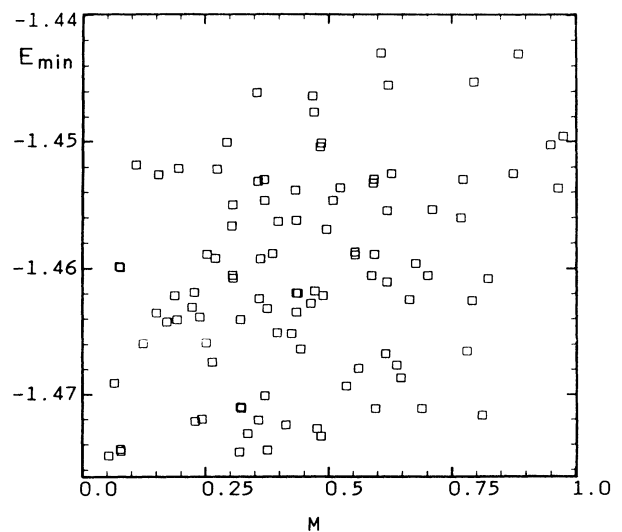


FIG. 1. The energies of 50 stationary states as a function of their magnetization. These states were obtained by starting the minimization of the energy from 50 different random initial conditions. Data for a 20×20 system with $\lambda = 0.5$ and $x = 0.2$.

fact that important morphological differences may exist between states that are essentially degenerate. It is clear that, to appropriately describe the $T=0$ properties of the model, we need to average physical quantities over those sets of quasidegenerate states whose energies lie near the (unknown) absolute minimum. However, as illustrated by Fig. 1, the energies of most of the configurations that one can reach by random generation lie far above the ground state and, to have enough low-energy data, one would need to generate huge numbers of them.

We found a more efficient way to reach the low-energy part of the spectrum based on the morphological properties of the stationary states. Figure 2 shows the configuration that corresponds to the lowest point in Fig. 1 at $E = -1.4749J$. The structure is characterized by the existence of ferromagnetically ordered domains in regions that are either relatively free of impurities or where impurities are isolated, surrounded by other regions where the density of frustrated plaquettes is high. Imagine now that we deform this configuration, denoted henceforth as the parent configuration, by rotating independently but rigidly the domains and giving arbitrary angles to the spins that belong to the boundaries between domains or, more generally, to a highly frustrated environment. If this configuration is used as the starting point of a new series of minimizations we may expect to generate states with energies lower than that of the parent state. The reason is that, by preparing the new initial state in this manner, the environment of those spins that were already in a high local field stays unchanged (except for a global rotation) whereas the spins that were in a weak local field have a chance to increase it.

We may implement this idea in practice by using the value of the internal field H_L acting on a spin as a criterion to decide whether and by how much to rotate it. This is because the features in the field distribution reflect the existing different spin environments in the sample.

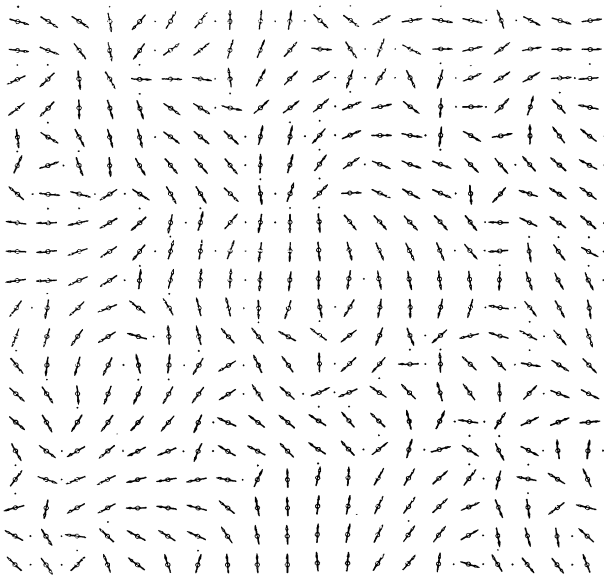


FIG. 2. Spin configuration in the state of lowest energy in Fig. 1. The dots indicate the positions of the impurity bonds.

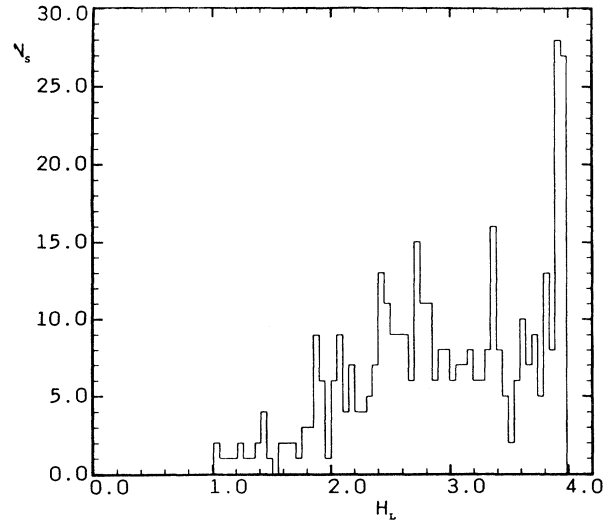


FIG. 3. Histogram showing the distribution of internal fields H_L in the spin configuration of Fig. 2.

As an example, the distribution of internal fields for the particular case of Fig. 2 is shown by the histogram in Fig. 3. The large peak for $3.8 \leq H_L \leq 4.0$ contains spins in the domains, the feature near $H_L = 2.5$ corresponds typically to spins that sit at one end of an isolated impurity bond. The more frustrated spins, those at the confluence of two impurity bonds, have local fields $H_L \leq 1.7$ and so on.

In one way of proceeding, we reinitialize the spins of the parent configuration assigning new, arbitrary angles to those spins whose local field H_L is less than a threshold H^* and impose small random deviations with respect to their previous equilibrium position to all the others. Then we let the system find a minimum, starting from this new initial condition. The procedure is repeated for different values of H^* , each of which leads to a new minimum.

Figure 4 shows the energies of the sequence of stationary states thus obtained as a function of H^* . Notice that, as expected, most of the new states have an energy lower than that of the parent state. The spin distribution of the state at $E = -1.507501J$, the lowest of the series, is shown in Fig. 5. Comparison between Figs. 2 and 5 shows that the domain structure of the parent and of the daughter states is basically the same but that the two configurations differ by large-scale collective rotations of the spins in the domains. It would have been extremely hard to generate one of these states starting from the other by using an algorithm where spins are updated one at a time.

To find states of even lower energy, we may use this configuration as a parent and generate a new set of minima by repeating the steps just described, and so on. This generates an arborescent structure that stops when we reach the point where every new state produced has an energy higher than that of its parent. At this point we estimate that we have reached the ground state.

To take degeneracy into account, we must compute the

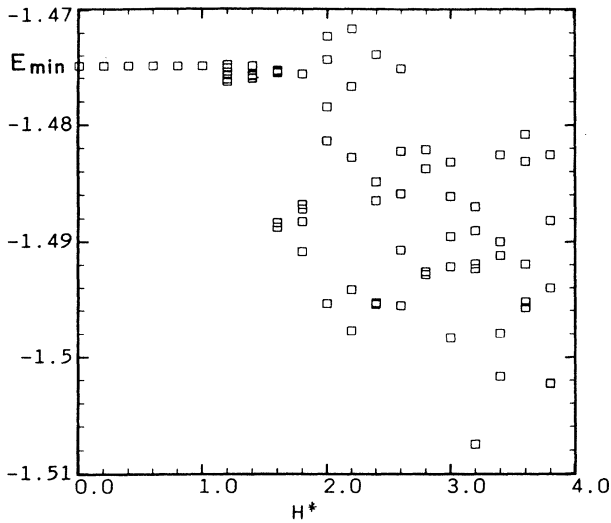


FIG. 4. Energy as a function of threshold field H^* . A point in the figure represents the energy of the stationary state reached by a minimization of the energy in which the starting configuration is derived from that of Fig. 2 by randomly initializing all the spins whose molecular field is less than H^* .

observable quantities as appropriate statistical averages over sets of states that lie near the ground state. Once the latter has been found we go backwards and collect the information about all the states in the hierarchy whose energies lie within a suitably defined window above the ground-state energy. The results of the next section have been obtained with data from the ground state and states with energy in a band of width $\Delta E \approx 10^{-5}J$ above it. This width corresponds to about ten times our uncertainty in the energies per spin. Typically, each parent state gives rise to about ten states within the allowed band.

It is interesting to see what the morphological

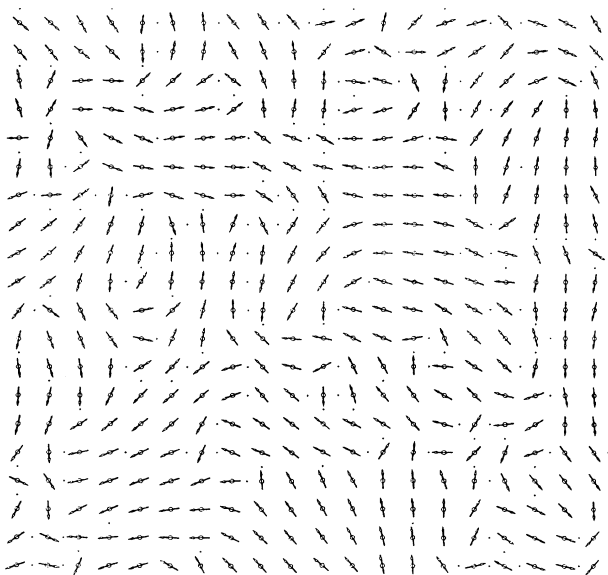


FIG. 5. Spin configuration in the state of lowest energy in Fig. 4.

differences are among pairs of states that contribute to the average. Often, but not always, the reason of almost degeneracy can be traced back to the kind of discrete symmetry mentioned in the Introduction. A particularly striking example is provided by Figs. 6(a) and 6(b) where we show part of two ground-state configurations of a 40×40 system with $\lambda=0.5$ and $x=20\%$. Within our accuracy, these are degenerate ($\Delta E \approx 10^{-7}J$). It can be

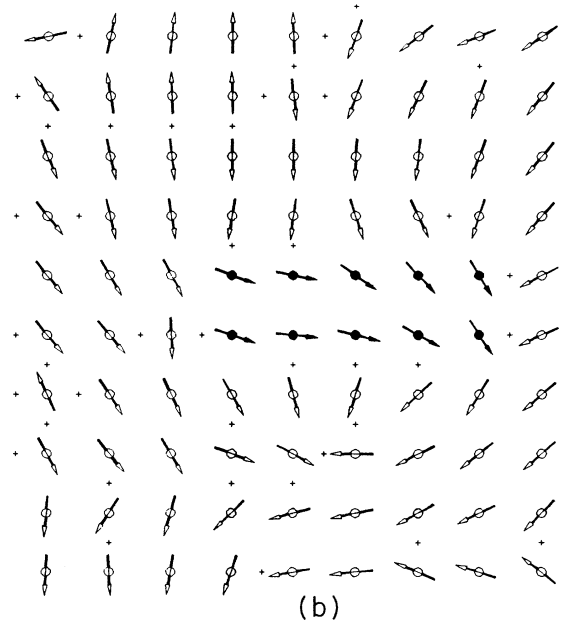
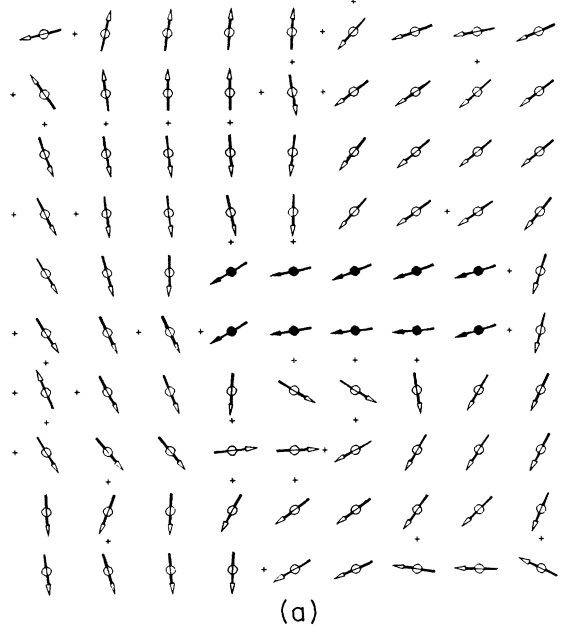


FIG. 6. Configuration of the same group of spins in two degenerate ground states of a 40×40 system with $\lambda=0.5$ and $x=20\%$. The bold spins belong to the domain to which reference is made in the text.

seen that the main features of Fig. 6(b) can be obtained from Fig. 6(a) by rotating the spins that belong to the domain on the right-hand side of the figure by π around a vertical axis. The rest of the spins are subject to relatively minor rearrangements.

III. RESULTS OF NUMERICAL CALCULATIONS

We have applied the method described above to the study of several systems corresponding to a wide range of concentrations and values of λ . In the following we describe in detail the results obtained for three representative values of λ and three sizes, 20×20 , 40×40 , and 80×80 . All along we have used periodic boundary conditions. The points in the curves represent averages over the sets of quasidegenerate states and five random configurations of bonds. We present the results for the order parameters first and then those for the correlation function.

A. Order parameters

Two order parameters characterize the possible ground states: the spontaneous magnetization

$$M = \left\langle \left| \frac{1}{N} \sum_{i=1}^N \mathbf{S}_i \right| \right\rangle_{\text{dis}} \quad (4)$$

and the Edwards-Anderson order-parameter tensor

$$Q_{\alpha\beta} = \frac{1}{N} \sum_{i=1}^N \langle \langle S_{i,\alpha} \rangle \langle S_{i,\beta} \rangle \rangle_{\text{dis}}. \quad (5)$$

In these expressions the angular brackets stand for an average over the set of quasidegenerate ground states. Before taking these averages we have removed from every configuration an arbitrary global spin rotation that is generally present as a consequence of the spin-rotation invariance of the Hamiltonian. We do this by uniformly shifting all the angles so that the magnetization \mathbf{M} points into some fixed direction, the same for all configurations (\mathbf{M} is never strictly zero in a finite system). This is the finite-size equivalent of the usual expedient of including the effect of an infinitesimal magnetic field in the Hamiltonian of the infinite system. Once all the angles are referred to a common origin:

$$Q_{\alpha\beta} = Q_L \hat{M}_\alpha \hat{M}_\beta + Q_T (\delta_{\alpha\beta} - \hat{M}_\alpha \hat{M}_\beta) \quad (6)$$

defining the transverse and longitudinal parts of the Edwards-Anderson order parameter.

A quantity useful for the characterization of the spin morphology is the noncollinearity,⁵

$$Q_{\text{NC}} = \left[\frac{2}{N^2} \sum_{i=1}^N \sum_{j=1}^N |\langle \mathbf{S}_i \rangle \times \langle \mathbf{S}_j \rangle|^2 \right]^{1/4}. \quad (7)$$

This is equal to zero for a collinear system and it is normalized such that it is equal to unity for a random angular distribution. In the XY model, Q_{NC} is not an independent quantity but is related to the Edwards-Anderson order parameter

$$Q_{\text{NC}} = (4Q_L Q_T)^{1/4}. \quad (8)$$

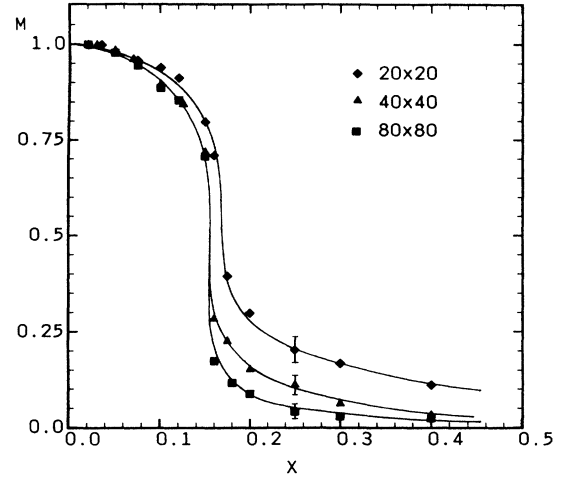


FIG. 7. The magnetization per spin M vs the concentration of impurities for $\lambda=0.5$. The points are actual data. The solid lines are guides for the eye.

We have studied a variety of values of λ and concentrations. The qualitative features of the concentration and size dependence of the order parameters differ according to whether λ is greater or smaller than 1. The results for values of λ that belong to the same group are similar. Thus, we only discuss in detail two cases, one on each side of $\lambda=1$.

We begin with the results for $\lambda=0.5$, representative of the case $\lambda \leq 1$. Figure 7 shows the magnetization as a function of concentration for this value of λ and three sample sizes. The curves suggest that the system undergoes a transition from a magnetic to a nonmagnetic ground state at a critical concentration $x_c \approx 15.5\%$. Notice that the magnetization starts to drop as soon as the concentration of impurities is finite. The obtention of this result, obvious from a physical point of view, is numerically nontrivial because, at low concentrations, the ferromagnetic state and the canted ground state lie extremely close in energy. For 1% of impurities, the energy differences are of the order of $10^{-6}J/\text{spin}$ which gives an idea of the accuracy necessary to handle this problem properly.

For this value of λ , the CPA instability is at $x \approx 2.5\%$. We conclude that this instability is not related to the transition to the nonmagnetic state. Near this concentration the magnetization begins to depart noticeably from the value $M=1$, giving some credit to the idea that the CPA line may qualitatively describe a crossover line.

We gather independent evidence in favor of the existence of a transition from the concentration dependence of the amplitude of the magnetization fluctuations,

$$\Delta M^2 = \frac{1}{N} \sum_i \langle \mathbf{S}_i \cdot \mathbf{S}_j \rangle - M^2. \quad (9)$$

As seen in Fig. 8, there is a peak in ΔM^2 at the same value of x_c at which the spontaneous magnetization tends to vanish. The height of the peak increases with the size of the system while its width decreases. However, its po-

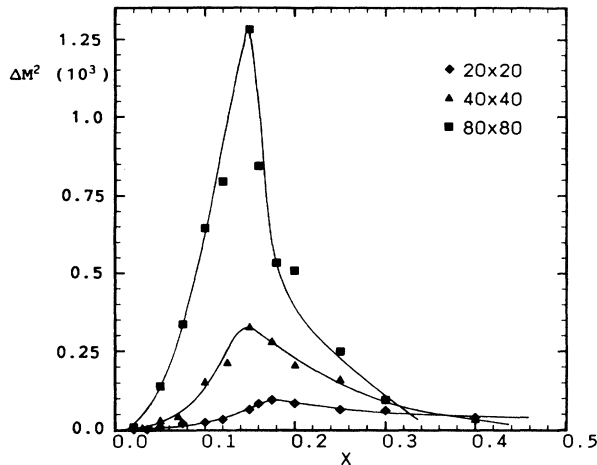


FIG. 8. Magnetization fluctuations ΔM^2 as a function of x for $\lambda=0.5$.

sition converges quickly to a limiting value independent of size.

To determine the nature of the two different phases, we computed the Edwards-Anderson order parameter. As shown in Fig. 9, the transverse and longitudinal components of $Q_{\alpha\beta}$ are different at low concentrations. Symmetry breaking can only occur in the presence of a finite spontaneous magnetization. Thus, the point at which $Q_{\alpha\beta}$ becomes isotropic may be identified with the transition point. Below x_c , Q_L decreases as the concentration of impurities increase since this component contains a contribution proportional to the square of the magnetization and this vanishes as $x \rightarrow x_c$. On the other hand, Q_T describes the frozen-in disorder of the component of the spin transverse to the finite magnetization and increases with the concentration of impurities. Beyond the transition point, the system is isotropic and the diagonal

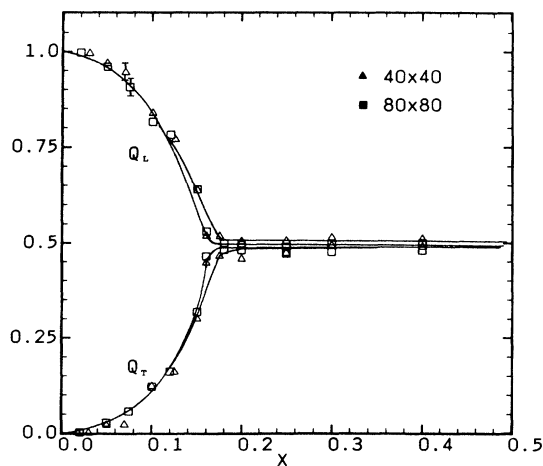


FIG. 9. Longitudinal (Q_L) and transverse (Q_T) components of the Edwards-Anderson order-parameter tensor for $\lambda=0.5$. The tensor becomes diagonal at the transition point.

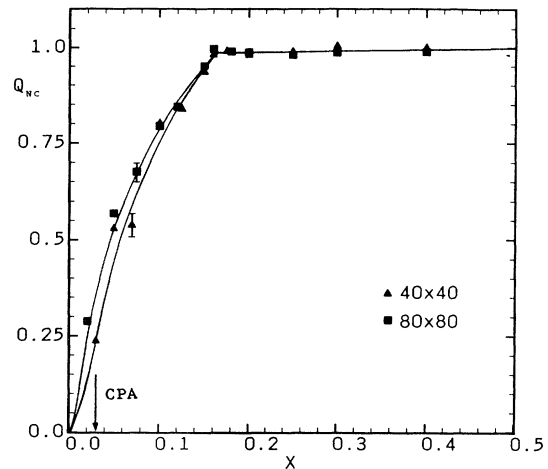


FIG. 10. Noncollinearity Q_{NC} as a function of concentration for $\lambda=0.5$. The arrow points at the CPA critical concentration.

Edwards-Anderson order parameter attains the value $\frac{1}{2}$ corresponding to a pure spin-glass phase at $T=0$.

A pictorial representation of the evolution of the morphology with concentration is provided by the x dependence of the noncollinearity defined by Eqs. (7) and (8) and shown in Fig. 10. Q_{NC} stays finite for all finite concentrations and vanishes in the limit $x \rightarrow 0$. The noncollinearity rises rather rapidly and reaches its maximum value in the vicinity of the transition point. For comparison, an arrow shows the concentration at which the CPA situates the onset of noncollinearity.

Convergence as a function of size becomes somewhat slower with decreasing λ but the results are otherwise similar. Figures 11 and 12 show the spontaneous magnetization and the Edwards-Anderson order parameter as a function of concentration for $\lambda=0.2$. The arrow points at the transition point as determined from the peak in the

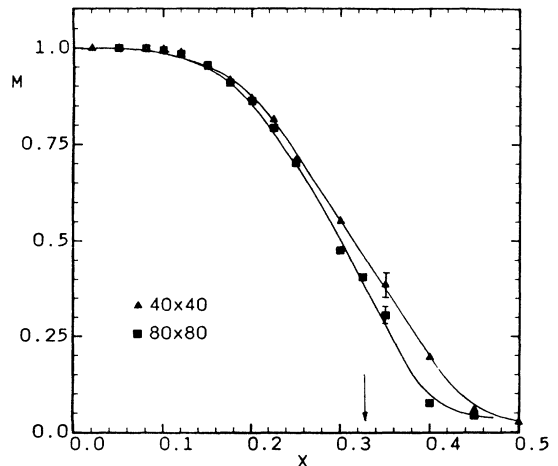


FIG. 11. Magnetization vs x for $\lambda=0.2$. Solid curves are guides for the eye. The arrow points at the position of the transition point as deduced from the magnetization fluctuations.

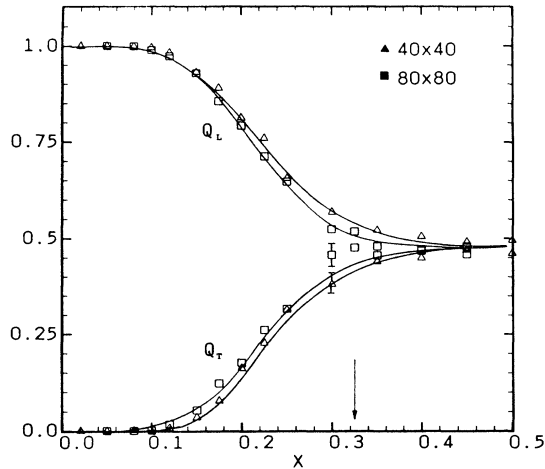


FIG. 12. Longitudinal and transverse components of the Edwards-Anderson order parameter vs x for $\lambda=0.2$. The arrow points at the position of the transition point.

magnetization fluctuations (cf. Fig. 13). One interesting effect of decreasing λ is that the transition region spreads over a wider range in concentration. This is clearly illustrated by the behavior of Q_{NC} (Fig. 14) that attains its maximum value much more gradually than in the previous case (cf. Fig. 10).

The $\lambda=3$ case is representative of the behavior for $\lambda \geq 1$. This is the region where isolated impurity bonds induce spin deviations. Simple heuristic arguments to be discussed in detail below suggest that, in this region, the system may be disordered for all $x \neq 0$. Figure 15 shows the magnetization as a function of x for $\lambda=3$ and various sizes. Comparison with Figs. 7 and 11 suggests that this case differs from the previous ones in that convergence as a function of the size is not at all apparent. The same lack of convergence is reflected by the curve of magnetization fluctuations in Fig. 16: the position of the peak in

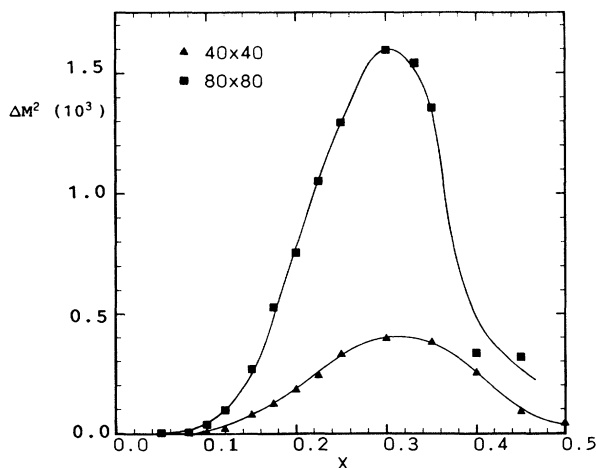


FIG. 13. Magnetization fluctuations ΔM^2 as a function of x for $\lambda=0.2$.

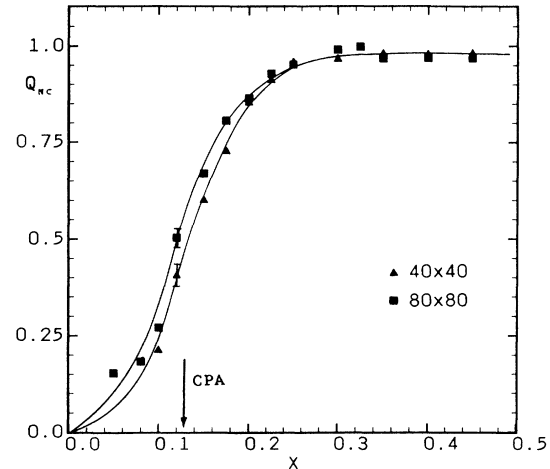


FIG. 14. Noncollinearity Q_{NC} as a function of concentration for $\lambda=0.2$. The arrow points at the CPA critical concentration.

ΔM^2 , that saturates rapidly as a function of size for $\lambda < 1$, seems to shift continuously to the left as the size increases for $\lambda=3$. This shift of the transition point is confirmed by the behavior of the Edwards-Anderson order parameter (Fig. 17). Notice that, in the previous cases this parameter was the one that showed the transition most clearly.

A tempting interpretation of this behavior, that we found for all $\lambda \geq 1$, is that, in the thermodynamic limit, the transition point is at $x=0$. This has the merit of being in agreement both with intuitive arguments and consistent with the results of the CPA.⁷ However, one cannot rule out the possibility that the two regimes are qualitatively identical and that the apparent difference is due to the fact that $x_c(\lambda)$ decreases very rapidly with increasing λ making finite-size effects more important for $\lambda \geq 1$. Studying samples of up to 80×80 sites, we have been un-

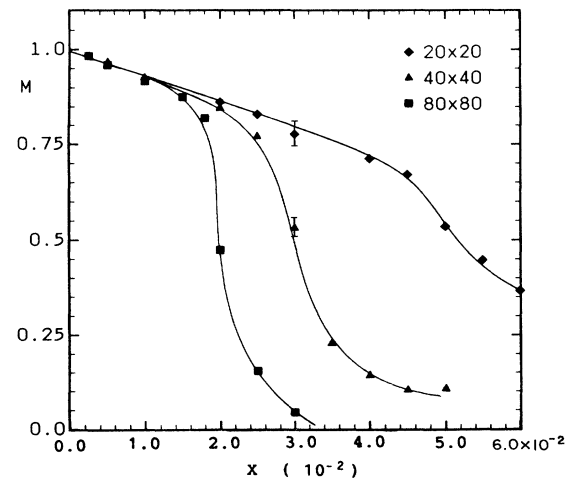


FIG. 15. The magnetization per spin M vs the concentration of impurities for $\lambda=3$.

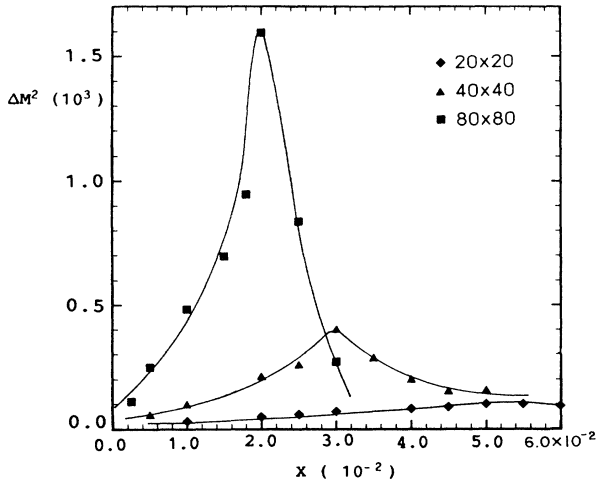


FIG. 16. Magnetization fluctuations ΔM^2 as a function of x for $\lambda=3$.

able to conclude unequivocally on this issue. Although we consider this possibility unlikely, to arrive at a definite conclusion we should study systems of sizes larger than the ones we have been able to attain.

B. Correlation functions

The spin-spin correlation function C_R ,

$$C_R = \frac{1}{N} \sum_{i=1}^N [\langle \mathbf{S}(\mathbf{R}_i + \mathbf{R}) \cdot \mathbf{S}(\mathbf{R}_i) \rangle]_{\text{dis}} \quad (10)$$

is isotropic and, for fixed size and λ , it depends qualitatively upon the impurity concentration. This is seen in Fig. 18(a) [18(b)] where we show C_R versus R for $\lambda=3$ and x smaller (larger) than the critical value x_c determined from the maximum in the fluctuations (Fig. 16).

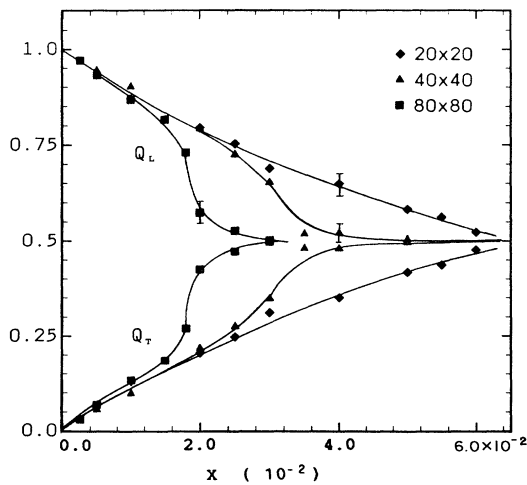


FIG. 17. Longitudinal and transverse components of the Edwards-Anderson order parameter vs x for $\lambda=3$.

The symbols represent actual data and the solid lines are fits to the functional forms to be discussed shortly.

The correlation function seems to change qualitatively as x crosses x_c in the sense that it is described by different analytic expressions on either side of x_c . We have found the same behavior for all values of λ . With varying λ , x_c and the fit parameters change, but the different sets of curves are, in all respects, similar. The fits are of very good quality in both regimes with dispersions in the range $\Delta\chi^2 \approx 10^{-5} - 10^{-6}$.

Not surprisingly, the fit in the “disordered region” ($x \geq x_c$), is of the form

$$C_R = A_+ \exp \left[-\frac{R}{\xi_+} \right] + B_+, \quad (11)$$

where A_+ , ξ_+ , and B_+ are determined by the fit. A_+ is

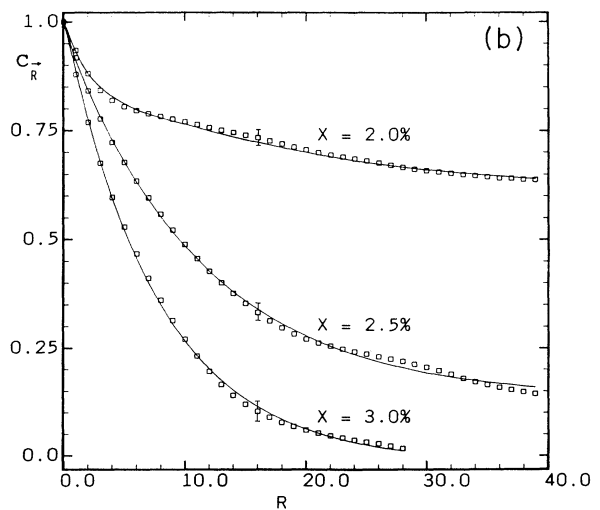
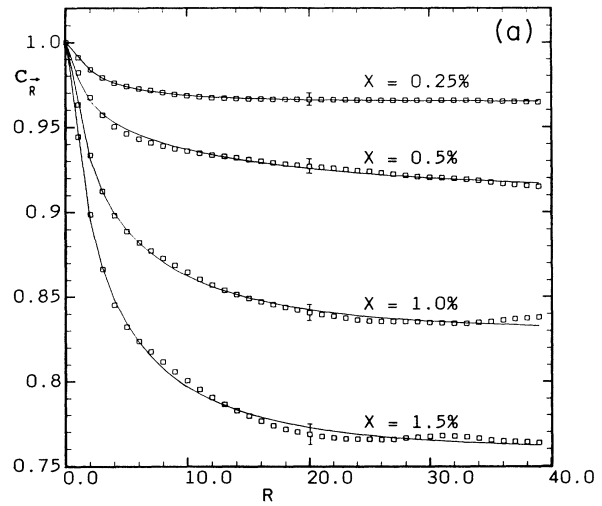


FIG. 18. Spin-spin correlation function C_R as a function of R for a 80×80 system with $\lambda=3$ for concentrations below (a) and above (b), the critical concentration. The squares denote the results of the numerical calculations. The solid curves are the fits described in the text.

almost size independent and varies smoothly when we vary λ or x . B_+ is expected to vanish in the thermodynamic limit. Although we found that it decreases with increasing size and that it is already very small for the 80×80 systems, we do not have enough data to describe in detail its size dependence. The typical behavior of the correlation length ξ_+ is shown in Fig. 19 for the $\lambda=0.5$ case. The correlation length increases as we approach x_c from the right and seems to converge well as a function of size. Obviously our data are insufficient to determine whether a divergence will develop at the critical point for the infinite system.

Our naive expectation was that the data in the "ordered" region ($x \leq x_c$) would be fitted by a similar expression

$$C_R = A_- \exp\left[-\frac{R}{\xi_-}\right] + B_- , \quad (12)$$

where, for infinite size, $B_- \rightarrow M^2$, the square of the ordered moment. It turns out, however, that this form cannot account for our results which are, instead, very well described by the formula

$$C_R = A_- \left[\frac{1}{\xi_-^2} + \frac{1}{R^2} \right]^{\beta/2} , \quad (13)$$

valid for $|\mathbf{R}| \geq a$, the lattice spacing.

A_- is a rather featureless amplitude but the exponent β has, on the contrary, a very interesting power-law dependence on density with an exponent that depends on λ . Several examples of this are plotted in Fig. 20. Referring to the cases shown in the figure, we find

$$\beta \propto \begin{cases} x, & \lambda=3, \\ x^2, & \lambda=0.5, \\ x^3, & \lambda=0.35, \\ x^4, & \lambda=0.2. \end{cases} \quad (14)$$

A simple heuristic argument can be given that explains

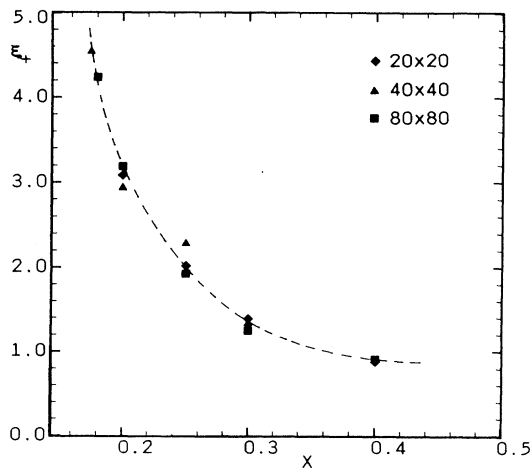


FIG. 19. Correlation length of the disordered phase as function of concentration for $\lambda=0.5$.

the emergence of a power law and the peculiar density dependence of β shown above. We begin by recalling first the argument¹³ that predicts the absence of long-range order for all $x \neq 0$ if $\lambda \geq 1$. In this case each individual impurity is the source of a dipolar distortion field. In a continuum description, the polarization in the medium is given by

$$\mathbf{P}(\mathbf{r}) = \sum_{i=1}^{N_{\text{imp}}} \mathbf{p}_i \delta(\mathbf{r} - \mathbf{r}_i) , \quad (15)$$

where \mathbf{r}_i is the position of the i th impurity bond and \mathbf{p}_i its dipole moment

$$\mathbf{p}_i = \mu \sigma_i \hat{\mathbf{e}}_i , \quad (16)$$

where μ , a function of λ , is the strength of the dipole, $\hat{\mathbf{e}}_i = \hat{\mathbf{x}}$ or $\hat{\mathbf{y}}$, is the direction of the bond, and σ_i its pseudo spin.

The angular pattern is the solution of

$$\nabla^2 \varphi(\mathbf{r}) = -2\pi \nabla \cdot \mathbf{P}(\mathbf{r}) . \quad (17)$$

Under the assumption that pseudospins do not order and are correlated over short distances, a brief calculation gives the asymptotic behavior

$$\langle [\varphi(\mathbf{r}) - \varphi(0)]^2 \rangle_{\text{dis}} \approx 2\pi \mu^2 \ln \left[\frac{r}{a} \right] \frac{N_{\text{imp}}}{N} \quad (18)$$

for $|\mathbf{r}| \gg a$. The logarithmic divergence in (18) has its origin in the dipolar nature of the long-distance distortion. The correlation function follows easily from (18),

$$C_r \approx \exp\left\{-\frac{1}{2} \langle [\varphi(r) - \varphi(0)]^2 \rangle\right\} \approx \left[\frac{a}{r} \right]^\beta \quad (19)$$

with the exponent $\beta = \pi \mu^2 x$, in agreement with the first entry in (14).

Since, when $\lambda \rightarrow 1$, $\mu \rightarrow 0$, single impurities are no longer a source of dipolar distortion for $\lambda < 1$. However, slightly more complicated clusters of impurities can lead

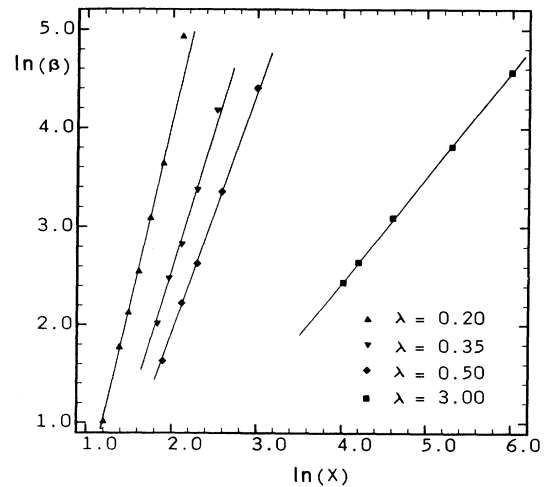


FIG. 20. log-log plot of the exponent β of formula (13) vs concentration x for several values of λ .

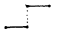
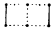
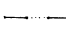



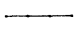
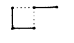

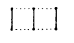
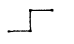
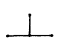
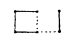
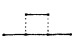

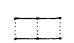



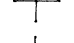
to the same effects. We have listed in Table I the thresholds and long-distance behavior of several clusters of two, three, and four impurities. Among the many arrangements that we have considered, the table includes those with the lowest thresholds. Several of the configurations in the list are sources of dipolar fields at long distances provided λ is above their respective thresholds that cover the whole interval (0,1). These are the most important impurity clusters because they are potential sources of logarithmic divergences in the region $\lambda \leq 1$. Whereas nondipolar clusters contribute to the degradation of the magnetic order too, they are always subdominant.

To understand the results in the region $\lambda < 1$ we must just look up in the table and see what the clusters are that are likely to be dominant at a given value of λ . We see that there is a dipolar cluster consisting of a pair of bonds at right angles with threshold below 0.5. For $\lambda = 0.5$, clusters like this, whose density is proportional to the square of the density, should be dominant and give rise to an exponent $\beta \propto x^2$ in agreement with (14). When we reach $\lambda = 0.35$, all two-impurity clusters are below threshold and we must begin to consider triplets in order to find possible dipolar sources. Since several are active at this value of λ , among them one that is listed in Table I, we can correctly deduce that, in this case, β should vary like x^3 . The last example is the $\lambda = 0.2$ case. We find one triplet that is still active at this value of λ (cf. Table I). However, this cluster is essentially at threshold, and its dipole moment $\mu_{\text{eff}} \approx 0$. As a result, it will only be important for very small values of x leaving the four-impurity clusters that are above threshold as the leading sources of disorder for $\lambda = 0.2$, thus explaining the last entry in (14).

These simple arguments predict a power-law decay of the correlations and do not give any hint of a mechanism that would explain the cutoff ξ_- that we need to include in order to fit our results. In part, the presence of a cutoff is due to our use of periodic boundary conditions which impose an artificial periodicity to the correlation function. However, we cannot exclude the existence of an intrinsic effect. A weak point in the above argument is that it neglects the interactions between the effective dipoles whose pseudospins are taken as independent random variables. In this approximation the possibility of screening of the dipolar fields at large distances is not considered. In the presence of screening, the power law would only hold up to distances of the order of the screening length which would thus be identified with ξ_- .

We have been unable to separate intrinsic and extrinsic contributions to ξ_- , a task that would require the analysis of samples much bigger than the ones we are able to handle because, in contrast with the previous case ($x \geq x_c$), ξ_- increases with (and is of the same order as) the size. We do not have data for a sufficient number of different sizes to decide whether ξ_- saturates with N or even to determine the existence of a tendency. Notice that this is in contrast with our previous findings that led us to the conclusion that, at least for $\lambda \leq 1$, convergence as a function of the size was satisfactory. There is, of course, no contradiction because the size dependence of different quantities need not be the same.

TABLE I. Instability thresholds for various clusters of two to four impurities. The third column indicates the nature of the distortions caused by the clusters at long distances: D =dipolar, Q =quadrupolar, L =localized.

Configuration	Instability threshold	Nature of distortions
—	1.0	D
	1.0	D
 or 	0.830	D or Q
 or 	0.571	D or Q
	0.467	D
	0.489	D
	0.455	D
	0.414	D
	0.393	D
	0.321	D
	0.199	D
	0.430	D
	0.384	D
	0.377	Q
	0.293	Q
	0.215	Q
	0.174	D
	0.171	D
	0.0	L

For the simple picture suggested by the results of Sec. III to hold, ξ_- should stay finite in the thermodynamic limit for $\lambda < 1$ where it should be related to the finite magnetization of the mixed phase by the relation $\langle |\mathbf{M}|^2 \rangle = A_- \xi_-^{-\beta}$. If, on the contrary, it turned out that $\xi_- \rightarrow \infty$ with the size, then we would arrive at a more exciting conclusion, namely, that the “ordered” phase is, in fact, a phase with power-law decay of correlations.

IV. CONCLUSION

We have developed an efficient and accurate method to study the phase diagram of the frustrated XY model at $T=0$. We have found that the main reason for the degradation of the magnetic order, at least at low concentrations, is the fact that some simple clusters of impurities are capable of creating long-range dipolar distortions once λ exceeds a certain threshold that depends on the size and shape of the cluster. The calculation of the

correlation functions shows this indirectly but quite clearly *via* the density dependence of the exponent describing incipient algebraic decay.

If one were to judge only on the basis of the results for the order parameters, one could make a good case for the existence of two different phases in the region $\lambda < 1$: a mixed phase for small concentrations, a spin-glass phase for higher doping. In the region $\lambda \geq 1$, the situation is not as clear because we are forced to reason on the basis of the observed *absence* of convergence up to the largest sizes that we have been able to consider. This is consistent with the simple arguments that predict a disordered state for all concentrations. However, in our opinion, this question remains far from settled.

The results for the correlation functions in the dilute region are puzzling because the modified power-law decay that we observe seems very unusual. The behavior of the correlation length throws some doubts on the validity of the simple picture described in the previous paragraph. One would need to study larger systems to determine accurately the size dependence of ξ_- in order to clearly

separate eventual intrinsic cutoff effects from finite-size ones. We cannot exclude the possibility of a divergence of ξ_- in the thermodynamic limit for *all* values of λ and x , in which case the transition that we observe would be one between two disordered phases, one with power-law decay of correlations, the other by exponential decay, just as in the case of the finite-temperature Kosterlitz-Thouless transition of the pure system.

ACKNOWLEDGMENTS

It is a pleasure to thank Thierry Dombre for the stimulus provided by his constant interest in this problem and for many valuable suggestions and comments. We also thank Jean Vannimenus for discussions on different aspects of this work and for his useful comments on the manuscript. The calculations reported in this work have been performed on the Cray 2 supercomputer of the Centre Grenoblois de Calcul Vectoriel du CEA. We thank their staff for technical help.

¹W. M. Saslow and G. N. Parker, Phys. Rev. B **38**, 11 733 (1988), and references cited therein.

²M. W. Dunlop and D. Sherrington, J. Phys. C **18**, 1465 (1985).

³L. R. Walker and R. E. Walstedt, Phys. Rev. B **22**, 3816 (1980).

⁴W. Kinzel and K. Binder, Phys. Rev. B **24**, 2701 (1981), and references cited therein.

⁵W. M. Saslow and G. N. Parker, Phys. Rev. Lett. **56**, 1074 (1986).

⁶A. Aharony, R. J. Birgeneau, A. Coniglio, M. A. Kastner, and H. E. Stanley, Phys. Rev. Lett. **60**, 1330 (1988).

⁷J. Vannimenus, S. Kirkpatrick, F. D. M. Haldane, and C.

Jayaprakash, Phys. Rev. B **39**, 4634 (1989).

⁸G. N. Parker and W. M. Saslow, Phys. Rev. B **38**, 11 718 (1988).

⁹J. Villain, J. Phys. C **10**, 1717 (1977).

¹⁰H. T. Diep, A. Ghazali, and P. Lallemand, J. Phys. C **18**, 5881 (1985).

¹¹M. Gulacsi and Zs. Gulacsi, Phys. Rev. B **33**, 3483 (1986).

¹²W. H. Press, B. P. Flannery, S. A. Teukolsky, and W. T. Vetterling, *Numerical Recipes* (Cambridge University, Cambridge, 1986).

¹³J. Villain, Z. Phys. B **33**, 31 (1979).